

# Gas sensor based on multiple Fano resonances in metal-insulator-metal waveguide resonator system

G. WAMG, Q. SHI, F. CHEN\*, Y. YU

*School of Physics and Optoelectronic Engineering, Yangtze University, Jingzhou, 434023, China*

A metal-insulator-metal (MIM) waveguide consisting of two stub resonators and a slot resonator is proposed, which can be used as gas sensor when the slot resonator is filled with poly-hexamethylene biguanide (PHMB) functional material. The primary principle is that the refractive index of the PHMB material is different when exposed to the  $CO_2$  with different concentrations. Finite difference-time domain (FDTD) simulation results show that the Fano resonance (FR) is originated from the coupling of the strong FP resonance and weak tooth cavity resonance, the Fano spectrum can be independently tuned by the geometrical parameters, it is also found that the FR 1, FR 3, FR4 can be tuned by the length of the stub resonator, and FR 2, FR5 are controlled by the length of the slot resonator. In addition, the FR positions (FR2 and FR5) are highly sensitive to the concentration of the  $CO_2$ . The sensitivity of the FR5 can be up to  $124 \text{ pm} / \text{ppm}$ . The sensitivity of the proposed plasmonic structure is about 9 times higher than reported in other similar sensors, which have possible future potential applications in slow light devices, nanoscale filters, and sensors for the detection of toxic gases.

(Received October 8, 2021; accepted August 10, 2022)

*Keywords:* Surface plasmon polariton, Metal-insulator-metal, Fano resonance, Gas sensor

## 1. Introduction

Surface plasmon polaritons (SPPs) are electromagnetic wave propagation along the metal-insulator interfaces, have attracted researchers focus due to it can overcome the traditional diffraction limit and the advantages of ultrafast optical signal processing ability [1-5]. SPPs have been applied to many platforms such as graphene nanophotonics, metal-insulator-metal (MIM) waveguide, photonic crystal structures and metamaterial structures [6-8]. MIM waveguide structure has been a hot spot since its strong local field capability, less expensive manufacturing cost and suitability for highly integrated circuits [9-10]. Recently, many MIM structures have been investigated numerically or theoretically, such as plasmonic switch, filters, nanosensor, plasmonic splitters and plasmonic Fano resonance[11-15].

Fano resonance shows excellent sensitivity to the change of environmental refractive index, which is

widely explored in all-optical switches, refractive index sensors and plasmonic modulators [16-22]. One approach to achieve Fano resonance is utilizing MIM waveguide, various structures have been proposed based on MIM waveguide to achieve single or multiple Fano resonance. For example, in 2021, Huo et al. proposed and studied tunable multiple Fano resonance and stable plasmonic band stop filter based on a MIM waveguide [23]. Chiang et al. studied multiple Fano resonance modes in an ultra-compact plasmonic waveguide-cavity system for sensing applications [24]. Guo et al. designed a MIM waveguide system with split ring resonator to achieve tunable triple Fano resonance [25]. Very recently, our group reported a plasmonic Fano sensor based on MIM waveguide resonator system with silver nanorod-defect [26]. People also proposed mechanisms analogous to Fano-resonant structures for sensing purpose, for example, Yun et al. reported a plasmonic system consists of a MIM stub resonator coupled with a plasmonic square cavity resonator, which possessed a sensitivity

938 nm/RIU and a maximum FOM  $1.35 \times 10^4$  [27]. Kazanskiy et al. numerically designed a PHMB coated metasurface perfect absorber for gas sensing with maximal sensitivity up to 17.3 pm/ppm [28]. In the field of experiment, Wang et al. designed a PHMB based Fabry-Perot interferometric optical fiber sensor for carbon dioxide gas sensing, a sensitivity of 12.2 pm/ppm is achieved [29].

Motivated by the work [27-29], in this paper, multiple Fano resonance is numerically realized in a compact plasmonic MIM waveguide system. The proposed structure is composed of two stub resonators and a slot resonator. By the numerical simulation based on the FDTD method, the transmission spectrum and magnetic field distributions are investigated in detail. The positions of FR1, FR3, FR4 peaks can be tuned by changing geometrical sizes such as the width and height of stub resonator, the positions of FR2, FR5 peaks can be tuned by changing geometrical sizes such as the width and height of slot resonator and coupling distance. When the slot resonator is filled with PHMB functional polymer, a sensitivity about 124 pm/ppm was obtained which is 9 times higher than the previously reported works. The proposed structure can be fabricated with lithography and deposition methods. The results of this paper have possible future potential applications in toxic gas sensors and refractive index sensors [30-33].

## 2. Model and theory

The proposed multiple Fano resonance is schematically depicted in Fig. 1, which consists of a MIM waveguide coupled with two stub resonators, and a side coupled slot resonator. The medium-purple part of the schematic diagram represents Ag and the white parts stand for air. The geometrical parameters are as follows:

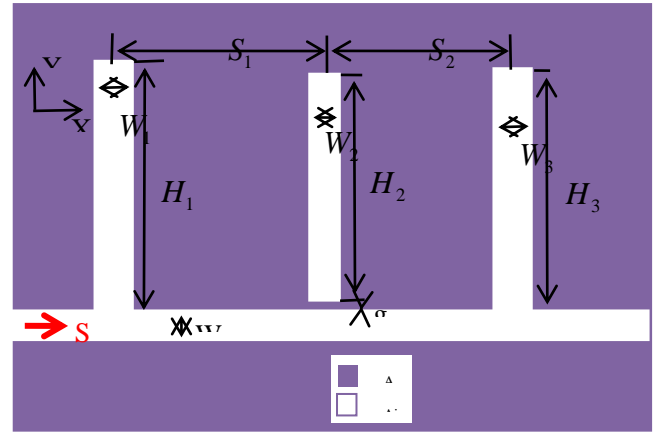


Fig. 1. 2D model of the proposed Fano resonance system with two stub resonators and a slot resonator (color online)

The heights and widths of the two stub resonators are labeled as  $H_1, H_3$  and  $W_1, W_3$ , the height and width of the slot resonator are  $H_2, W_2$ , and the coupling distance between the slot resonator and bus waveguide is  $g$ . The lengths between the left stub and the bus waveguide is  $S_1$ , the lengths between the right stub and the bus waveguide is  $S_2$ . The width of the bus waveguide is  $w = 50 \text{ nm}$  to ensure only fundamental mode exists in the waveguide. The metal is silver whose frequency-dependent complex relative permittivity is characterized by the drude model:

$$\epsilon_{Ag}(\omega) = \epsilon_{\infty} - \frac{\omega_p^2}{\omega^2 + i\omega\gamma_p} \quad (1)$$

where  $\epsilon_{\infty}$  is the dielectric constant at the infinite frequency,  $\omega_p$  and  $\gamma_p$  stand for the bulk plasmon frequencies and the electron collision, respectively. The parameters for silver can be set as  $\epsilon_{\infty} = 3.7$ ,  $\omega_p = 9.1 \text{ eV}$ , and  $\gamma_p = 0.018 \text{ eV}$  [34],  $\omega$  is the angular frequency of the incident light field. The grid sizes in 2D directions are set to be  $3 \text{ nm} \times 3 \text{ nm}$ ,  $\Delta t = \frac{\Delta x}{2c}$ , where  $c$  is the free space speed of light. The total simulation area is  $1800 \text{ nm} \times 1200 \text{ nm}$ , a plane wave source located in the bus waveguide from left to right is used for exciting

SPPs, and a power monitor is placed at the output port to obtain the transmission. Perfectly matched layers (PMLs) and metal boundary conditions are applied in the  $X$  direction and  $Y$  directions, respectively. For the proposed MIM coupled resonators system, the sensing performance is investigated by analyzing the resonance wavelength shifts. According to the standing wave theory, the resonators can be regarded as Fabry-Perot (FP) resonator, the resonance condition of FP resonator can be given by:

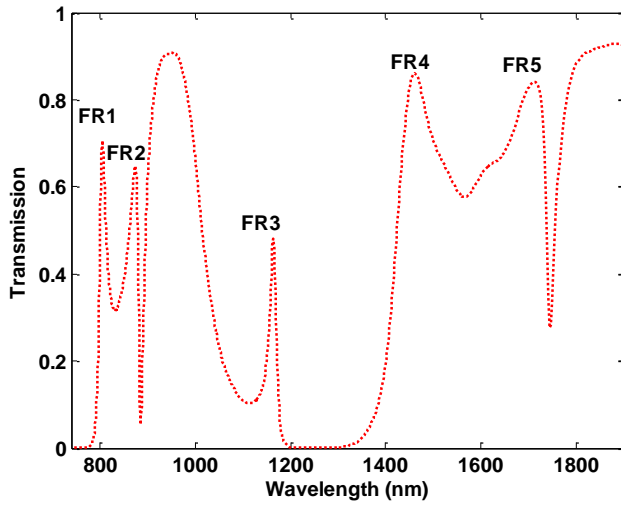


Fig.2. The transmission spectra of the coupled plasmonic system calculated by FDTD. (The geometrical parameters were set as  $w = 50$  nm,  $g = 20$  nm,  $W_1 = 90$  nm,  $W_2 = 70$  nm,  $W_3 = 90$  nm,  $H_1 = 725$  nm,  $H_2 = 615$  nm,  $H_3 = 725$  nm,  $S_1 = 640$  nm and  $S_2 = 550$  nm) (color online)

$$\lambda_m = 2\text{Re}(n_{\text{eff}})L_{\text{eff}} / m, m = 1, 2, 3, \dots \quad (2)$$

where  $m$  represents the order of the resonance mode,  $L_{\text{eff}}$  and  $n_{\text{eff}}$  stand for the effective resonance length and effective refractive index, the effective refractive index  $n_{\text{eff}}$  can be obtained from the dispersion relationship [35-36].

Fig. 2 shows the transmission spectra with  $w = 50$

nm,  $g = 20$  nm,  $W_1 = 90$  nm,  $W_2 = 70$  nm,  $W_3 = 90$  nm,  $H_1 = 725$  nm,  $H_2 = 615$  nm,  $H_3 = 725$  nm,  $S_1 = 640$  nm and  $S_2 = 550$  nm. It can be noticed that five Fano resonances (labeled by FR1, FR2, FR3, FR4, and FR5) at the resonant wavelength of  $\lambda_1 = 804$  nm,  $\lambda_2 = 873$  nm,  $\lambda_3 = 1165$  nm,  $\lambda_4 = 1461$  nm,  $\lambda_5 = 1715$  nm. One can see that the transmittance can sharply decrease from peak to dip. The wavelength shifts are about 8 nm, 37 nm, 23 nm for FR 1, FR2, and FR3, respectively. To further investigate the internal principle of the Fano resonance, we studied the steady-state magnetic-field

$|H_z|$  distributions. It can be noticed that the two stub resonators matter the five Fano resonances. Fig. 3 (a) shows the field intensity distribution at resonant wavelength 804 nm (FR1 peak), it can be noticed that magnetic-field distributions confined in the bus waveguide between two stub resonators, three antinodes are found in the bus waveguide. As shown in Fig 3 (c), two antinodes are found in the bus waveguide, while for Fig 3 (d), only one antinode is found. As shown in Fig 3 (f), the SPPs are blocked by the left stub resonator, no SPPs can pass to the output port. Therefore, FR 1, 3, 4 are result from the coupling of the strong FP resonance and weak tooth cavity resonance. As shown in Fig 3 (b), (e), at FR2 and FR 5, most part of the magnetic-field is confined in the slot resonator. These characteristics indicate that FR2 and FR 5 are originated from the coupling of bus waveguide and the slot resonator. Therefore, the resonant wavelengths of the FR2 and FR 5 can be controlled by the geometrical parameters of the slot resonator.

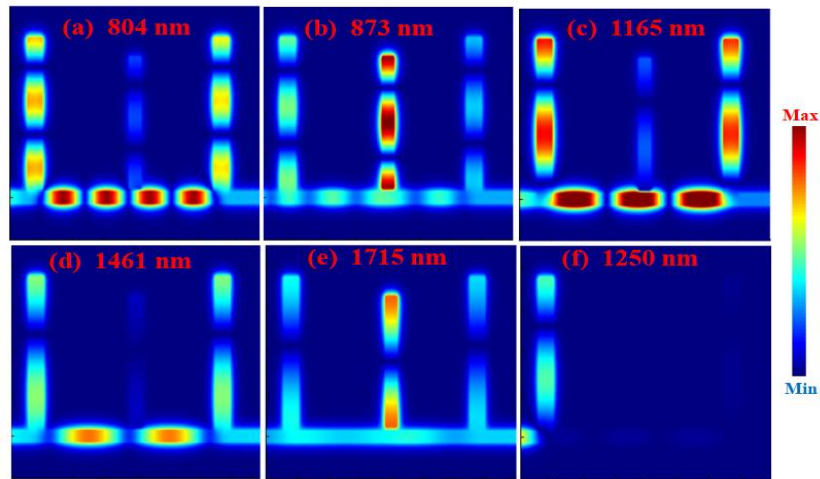
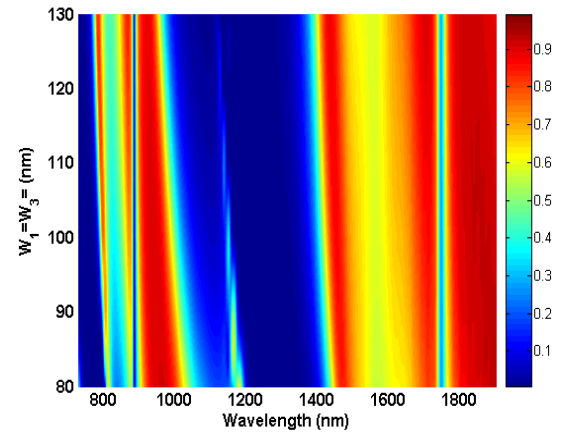


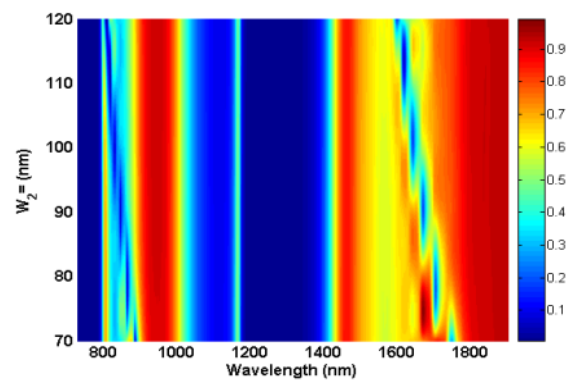
Fig. 3. Contour profiles of the magnetic-field  $|H_z|$  (a) FR1 at 804 nm (b) FR2 at 873 nm (c) FR3 at 1165 nm (d) FR4 at 1461 nm. (e) FR5 at 1715 nm (f) 1250 nm (color online)

The influence of stub resonator width  $W_1$  on the transmittance of the proposed structure is then investigated. As shown in Fig. 4 (a), when the width  $W_1$  ( $W_3$ ) increases from 80 nm to 150 nm, it can be seen that the resonant wavelengths of FR1, FR3 and FR4 are blue-shifted, but the resonant wavelengths of FR2 and FR5 kept unchanged. Fig. 4 (b) shows the transmittance spectra of the proposed structure with various  $W_2$ , when  $W_2$  increases from 70 nm to 120 nm, the resonant wavelength of FR1, FR3 and FR4 are have not changed, but the resonant wavelength of FR2 and FR5 are blue shifted. Therefore, we can tune the FR resonant wavelength independently by changing the width of the stub resonator and slot resonator.

In succession, we also investigated the effect of stub resonator heights  $H_1$ ,  $H_3$  on the transmittance spectra, As shown in Fig. 5(a), it can be seen that when the height of the stub resonator increases from 680 nm to 800 nm, the resonant wavelengths of FR2 and FR5 remain unchanged, but the resonant wavelengths of FR1, FR3, FR4 display blue-shifted. Fig. 5 (b) shows the transmittance spectra with different  $H_2$ , it can be seen that when  $H_2$  increases from 585 nm to 660 nm, the resonant wavelengths of FR1, FR3, FR4 keep unchanged, but the resonant wavelengths of FR2, FR5 display blue-shifted. Therefore, we can also tune the FR resonant wavelength independently by changing the height of the stub resonator and slot resonator.



(a)

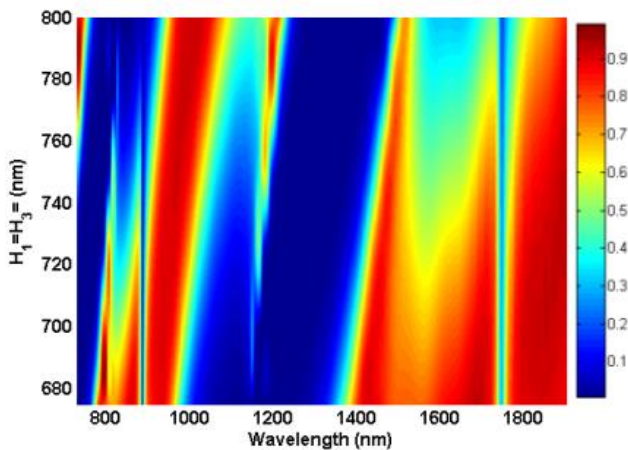


(b)

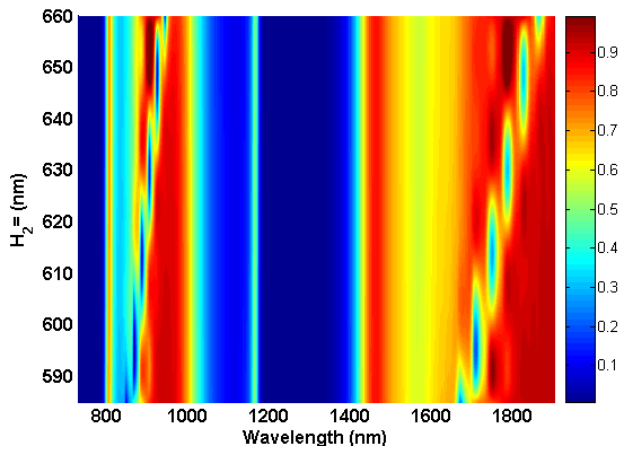
Fig. 4. The transmission spectra of the plasmonic Fano system with different  $W_1$ ,  $W_3$  and  $W_2$  (color online)

The effect of horizontal distance  $S_1$  and  $S_2$  on the transmittance is studied in details. As shown in Fig. 6 (a), (b), when  $S_1$  ( $S_2$ ) increases from 580 nm (510 nm) to 680

nm (610 nm) and the other parameters remained changeless, it can be seen that the resonant wavelengths of FR1, FR3 and FR4 are red shifted, but the resonant wavelengths and resonance intensities of FR2 and FR5 are have no apparent changes. The transmission of the MIM waveguide with different coupling distances  $g$  is shown in Fig 6 (c), when  $g$  increases from 20 nm to 70 nm, the resonance positions of FR1, FR3, FR4 are almost kept unchanged, when  $g$  increases to 70 nm, a blueshift happened to the FR2 and FR5, the FWHM (full width at half maximum of the transmission spectra) got smaller and the transmittance got higher. When  $g$  is bigger than 60 nm, FR2, FR5 resonances disappeared, since the coupling between the slot resonator and bus waveguide is so weak, and the slot resonator will no longer participate in the FR resonance.



(a)



(b)

Fig.5. (a) The transmission spectra of the proposed plasmonic Fano system with changing  $H_1$ ,  $H_3$  from 675 nm to 800 nm. (b) The transmission spectra of the proposed plasmonic Fano system with varying  $H_2$  from 585 nm to 660 nm (color online)

Fig. 7 (a) shows the schematic representation of plasmonic gas sensor when the slot resonator is filled with functional polymer material, due to the sharp transmission line shape, a high temperature sensitivity of the proposed structure can be achieved. To achieve high sensitivity, we use polyhexamethylene biguanide (PHMB) for sensitive to low concentrations of  $CO_2$  gas at room temperature and atmospheric pressure. Considering that PHMB material absorb and release of  $CO_2$  gas do not require the application of water vapor, it is an excellent candidate for the design of gas sensor. [37] The refractive index of the PHMB material with different  $CO_2$  gas concentrations can be extrapolated from the paper [38]. The length of the slot resonator is set as 405 nm, the other geometrical parameters are the same with Fig 2. It can be seen that FR2, FR5 are blue shift with increasing the  $CO_2$  gas concentration, while the positions of FR1, FR3, FR4 are almost unchanged. This is because the refractive index of the PHMB material decreases as  $CO_2$  gas concentration increases, then the effective index of slot resonator decreases. Fig. 7 (c) shows the Fano resonant wavelength with different gas concentrations. Fig. 7 (b) and (c) prove again that the slot resonator decides the position of FR2 and FR5.

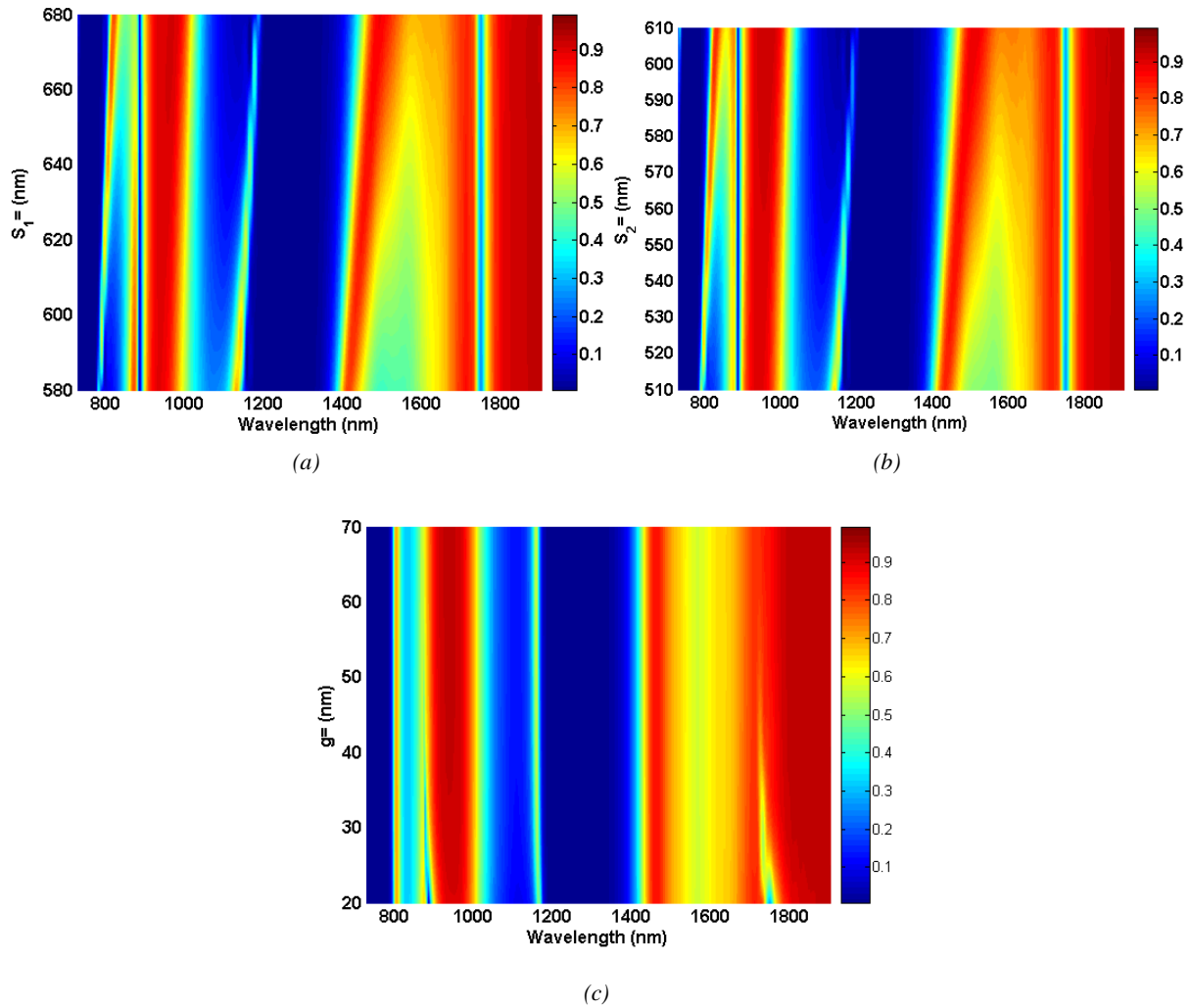


Fig. 6. Influence of parameters (a)  $S_1$  (b)  $S_2$  (c)  $g$  on the transmission characteristics of the proposed plasmonic Fano system (color online)

In sensing application, a high sensitivity is always designed. The sensitivity of the proposed plasmonic gas sensor can be defined as the shift of the FR peak with respect to the change in the gas concentration,  $S = d\lambda/dconc. (pm/ppm)$ . As depicted in Fig. 7 (b), when the gas concentration increased, the transmission spectra showed a remarkable shift. Fig. 7 (d) shows the sensitivity versus gas concentration, the sensitivity are approximately 51 pm/ppm, 124 pm/ppm at FR2, FR5,

respectively. The sensing performance of other related structures are compared and the results are shown in Table 1. The sensitivity of the present multiple Fano resonance structure is relatively good compared to other related work [39-42]. It is worth noting that, compared with the reference [37], the sensitivity of the structure proposed in this paper still have room for improvement when the structure is further optimized.

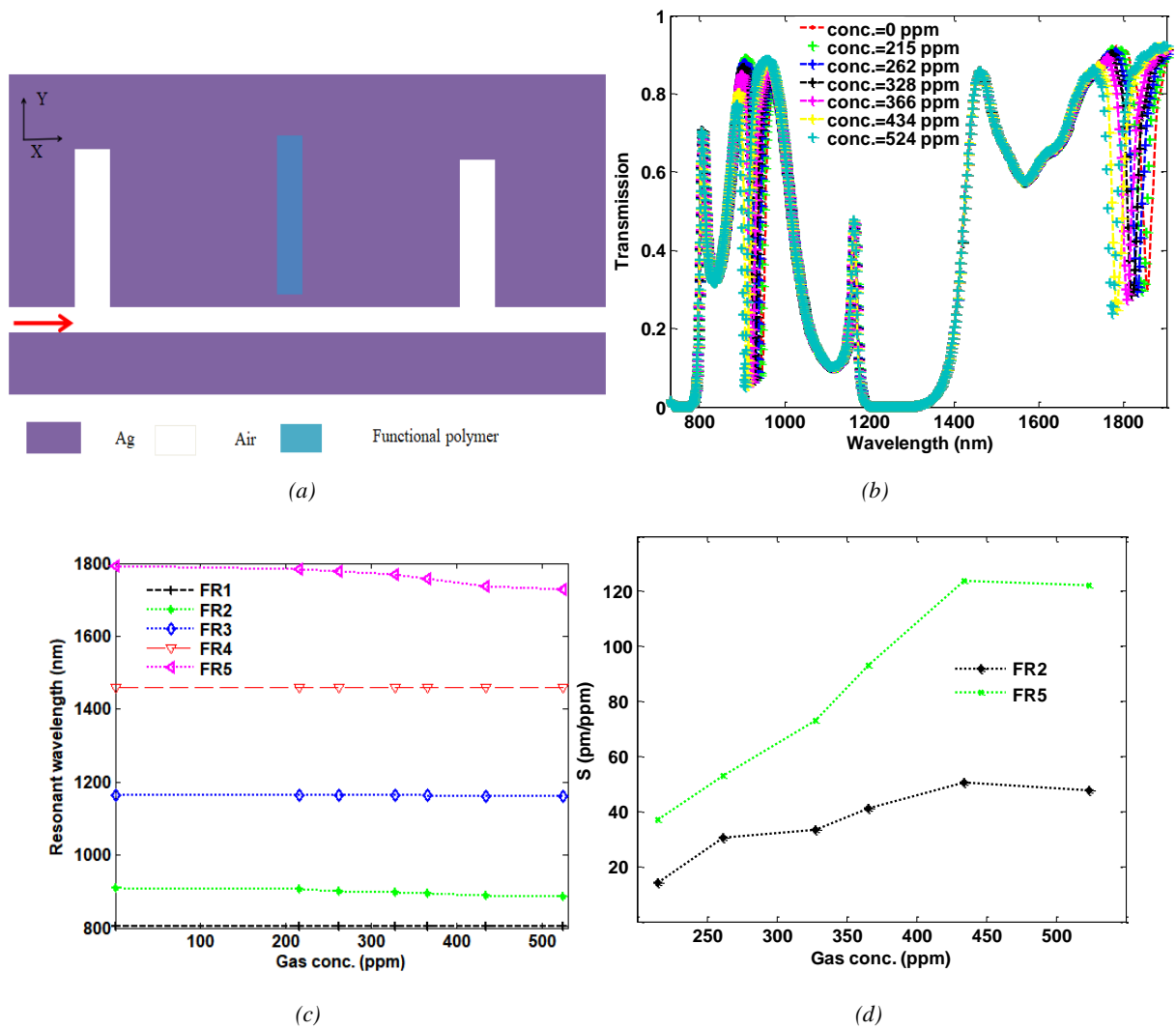


Fig. 7. (a) Schematic representation of plasmonic gas sensor when the slot resonator is filled with functional polymer (b) The transmission spectra for different gas concentration, when the length of slot resonator is 405 nm (c). The Fano resonant wavelength with different gas concentrations. (d) Sensitivity versus gas concentration (color online)

Table 1. Comparison with other plasmonic sensors

Structure in other work	Reference	Sensitivity (pm/ppm)
Stub waveguide coupled slot resonator	This work	124
Fabry diode gas detection	Ref 28	17.3
Optical fiber Fabry-Perot interferometric	Ref 29	12.2
Silicon subwavelength grating slot waveguide	Ref 41	12.9
MIM waveguide coupled ring resonator	Ref 42	28

### 3. Conclusion

In conclusion, multiple Fano resonance is numerically realized in a compact plasmonic MIM waveguide system. The proposed structure is composed of two stub resonators and a slot resonator. Then a plasmonic  $CO_2$  gas sensor is designed based on the slot resonator filled with a PHMB polymer material. Results show that five Fano resonances can be independently tuned by the geometrical parameters, such as the height or the width of stub resonators and slot resonator, horizontal distance between the two stubs and the center slot resonator. Based on FDTD simulation, a sensitivity

about 124 pm/ppm was obtained, which is about 9 times higher than the previously reported works based on MIM waveguide or metamaterials structure. The designed MIM waveguide structure can be applied not only in multiple Fano resonance, but also in toxic gas sensor by utilizing different polymer functional materials.

### Acknowledgements

Supported by The Yangtze Youth Fund (Grant No. 2016cqn55), Yangtze Fund for Youth Teams of Science and Technology Innovation (Grant No. 2015cqt03) . National Natural Science Foundation of China (Grant No. 11747091). Supported by the talent and high level thesis cultivation program of School of physics and Optoelectronics Engineering, Yangtze University.

### References

- [1] J. Tao, X. G. Huang, X. S. Lin, Q. Zhang, X. P. Pin, *Opt. Express* **17**, 13989 (2009).
- [2] H. Raether, *Surface plasmon on smooth surfaces and on gratings*, Springer, Berlin, Heidelberg, 4 (1988).
- [3] F. Chen, H. F. Zhang, L. H. Sun, J. J. Li, C. C. Yu, *Opt. Laser Technol.* **116**, 293 (2019).
- [4] P. Neutens, P. Van Dorpe, I. De Vlainck, L. Lagae, G. Borghs, *Nat. Photonics* **3**, 283 (2009).
- [5] D. K. Gramotnev, S. I. Bozhevolnyi, *Nat. Photonics* **4**, 8 (2010).
- [6] H. Lu, X.T. Gan, D. Mao, B. H. Jia, J. L. Zhao, *Scientific Reports* **8**, 1558 (2018).
- [7] Q. Yang, X. B. Liu, F. Q. Guo, H. N. Bai, B. H. Zhang, X. Lin, Y. Tan, Z. Zhang, *Optik* **220**, 165163 (2020).
- [8] F. Chen, *J. Mod. Optic* **64**, 1531 (2017).
- [9] Z. Chen, J. J. Chen, L. Yu, J. H. Xiao, *Plasmonics* **10**, 131 (2015).
- [10] J. Chen, C. Sun, Q. Gong, *Opt. Lett.* **39**, 52 (2014).
- [11] G. Zhang, R. Liang, H. Liang, J. Luo, R. Zhao, *Opt. Express* **22**, 9912 (2014).
- [12] X. Ren, K. Ren, Y. Cai, *Appl. Opt.* **56**, H1 (2017).
- [13] X. S. Lin, X. G. Huang, *J. Opt. Soc. Am. B* **26**, 1263 (2009).
- [14] T. Nikolajsen, K. Leosson, S. Bozhevolnyi, *Appl. Phys. Lett.* **85**, 5833 (2004).
- [15] H. Lu, X. Liu, D. Mao, G. Wang, *Opt. Lett.* **37**, 3780 (2012).
- [16] T. Nurmohammadi, K. Abbasian, R. Yadipour, *Opt. Commun.* **410**, 142 (2018).
- [17] Y. Karimi, H. Kaatuzian, A. Tooghi, M. Danaie, *Optik* **243**, 167424 (2021).
- [18] A. K. Paul, M. S. Habib, N. H. Hai, S. M. A. Razzak, *Opt. Commun.* **464**, 125556 (2020).
- [19] H. X. Han, D. L. Hou, L. Zhao, N. N. Luan, L. Song, Z. H. Liu, Y. D. Lian, J. F. Liu, Y. S. Hu, *Sensors* **20**, 1009 (2020).
- [20] Q. W. Ye, L. Y. Guo, M. H. Li, Y. Liu, B. X. Xiao, H. L. Yang, *Phys. Scripta* **88**, 055002 (2013).
- [21] M. Danaie, H. Kaatuzian, *Photonics Nanostruc. Fundam. Appl.* **9**, 70 (2011).
- [22] J. Chen, H. Nie, C. J. Tang, Y. H. Cui, B. Yan, Z. Y. Zhang, Y. R. Kong, Z. J. Xu, P. G. Cai, *Appl. Phys. Express* **12**, 052015 (2019).
- [23] C. Zhou, Y. P. Huo, Y. Y. Guo, Q. Q. Niu, *Plasmonics* **10**, 1007 (2021).
- [24] C. T. C. Chao, Y. F. C. Chau, H. P. Chiang, *Results in Physics* **27**, 104527 (2021).
- [25] C. H. Wu, Z. C. Guo, S. X. Chen, J. Yang, K. H. Wen, *Results in Physics* **27**, 104508 (2021).
- [26] F. Hu, F. Chen, H. F. Zhang, L. H. Sun, C. C. Yu, *Optik* **229**, 166237 (2021).
- [27] B. F. Yun, G. H. Hu, R. H. Zhang, Y. P. Cui, *J. Opt.* **18**, 1 (2016).
- [28] N. L. Kazanskiy, M. A. Butt, S. N. Khonina, *Sensors* **21**, 378 (2021).
- [29] W. Ma, J. Xing, R. Wang, Q. Rong, W. Zhang, Y. Li, J. Zhang, X. Qiao, *IEEE Sensors J.* **18**, 1924 (2018).
- [30] F. Chen, H. F. Zhang, L. H. Sun, J. J. Li, C. C. Yu, *Optik* **185**, 585 (2019).
- [31] J. R. Mejía-Salazar, O. N. Oliveira, *Chem. Rev.* **118**, 10617 (2018).
- [32] S. F. Pang, Y. P. Huo, Y. Xie, L. M. Hao, *Opt. Commun.* **381**, 409 (2016).
- [33] B. Zeng, Y. Gao, F. J. Bartoli, *Nanoscale* **7**, 166 (2015).

- [34] H. S. Sehmi, W. Langbein, E. A. Muljarov, *Phys. Rev. B.* **95**, 115444 (2017).
- [35] Q. Zhang, X. G. Huang, X. S. Lin, J. Tao, X. P. Jin, *Opt. Express* **17**, 7533 (2009).
- [36] F. Hu, H. Yi, Z. Zhou, *Opt. Express* **19**, 4848 (2011).
- [37] S. N. Khonina, N. L. Kazanskiy, M. A. Butt, *Opt. Express* **11**, 16584 (2021).
- [38] K. P. Koushik, S. Malathi, *Networking and Computers* **649**, 157 (2020).
- [39] H. Li, B. Sun, Y. Yuan, J. Yang, *Opt. Express* **27**, 1991 (2019).
- [40] G. Mi, C. Horvath, M. Aktary, V. Van, *Opt. Express* **24**, 1773 (2016).
- [41] S. H. Badri, *Opt. Laser Technol.* **136**, 378 (2021).
- [42] M. Mansouri, A. Mir, A. Farmani, *Journal of Optoelectrical Nanostructures* **4**, 29 (2019).

---

\*Corresponding author: 501110@yangtzeu.edu.cn